Digital Signal Processing **12**, 159–174 (2002)
doi:10.1006/dspr.2002.0446

Applications of Smart Antennas to Rotorcrafts

Moeness Amin,* Yimin Zhang,* Vincent Mancuso,† and Ahmad Hoorfar*

*Department of Electrical and Computer Engineering, Villanova University, Villanova, Pennsylvania 19085; and †Boeing Helicopter Division, Mail Stop P32-21, P.O. Box 16858, Philadelphia, Pennsylvania 19142-0858
E-mail: moeness@ece.vill.edu, yimin@ieee.org, vincent.mancuso@phl.boeing.com, hoorfar@ece.vill.edu

Amin, M., Zhang, Y., Mancuso, V., and Hoorfar, A., Applications of Smart Antennas to Rotorcrafts, *Digital Signal Processing* **12** (2002) 159–174.

Transmitted and received signals involving rotorcrafts are subject to intermodulations caused by the rotor blades. In this paper, the statistical characteristics of the wireless communication link between a rotorcraft transmitter and a receiver on the ground are developed. Both the scattering and Doppler effects of the rotating blades on the impairment of frequency modulated frequency hopping signals are considered. The channel model includes the near-field wave propagation between the transmitter antenna and the scattering blades. The channel model is used to examine the performance of different diversity techniques, namely, the transmitter diversity, multicarrier frequency hopping, and the fast frequency hopping, in view of antenna polarization and relative strength of the direct path and the scattering component from the rotating blades.

Key Words: smart antenna; diversity technique; scattering; multipath fading; rotating blade; Doppler effect; transmitter diversity; multicarrier frequency hopping; fast frequency hopping.

1. INTRODUCTION

Rotorcrafts have been increasingly playing a major role in the digital battlefield. Without a reliable communication link, there could be a breakdown in command and control between the rotorcraft and the ground support. Reliability of the communication link is constantly degraded by Doppler effects caused by the rotation of the rotorcraft blades. In this paper, the Doppler effects on a communication link between a rotorcraft transmitter and a receiver on the ground are studied. The communication link of interest is at VHF where voice signals are transmitted at the frequency band of 30–88 MHz using multilevel FM modulation with frequency hopping (FH) schemes. Different

1051-2004/02 $35.00

diversity techniques are considered as solutions for mitigating the fading of the channel.

The communication system consists of a ground transceiver and rotorcraft transceiver. The ground transceiver consists of a signal receiver and a single antenna. The rotorcraft transceiver consists of a radio with one antenna or two spatially separated antennas.

A rigorous model that involves the near-field effects between the closely separated transmitter antennas and the rotating blades is developed. The channel model also includes the Doppler effect and the continuous position change of the rotating blades. The model reveals that various parameters in the underlying problem, specifically the rotor rotational signatures, produce a highly time-varying channel. The channel fading characteristics require the use of diversity techniques to effectively combat the channel impairment, maintain a desirable signal-to-noise ratio (SNR), and reduce outages.

The receiver diversity techniques with the use of multiple receiver antennas have been well developed. Herein, we focus on the link where the communication flow is from the single- or multiantenna rotorcraft to the single-antenna ground systems. In particular, we consider transmitter diversity, fast frequency hopping (FFH), and multicarrier frequency hopping (MCFH) diversity techniques to mitigate the channel fading. The improved performances of these methods are demonstrated using the receiver signal power.

2. SIGNAL MODEL

2.1. Signal Model

Figure 1 shows the block diagram of an FH/FM communication system. At the transmitter, the voice signal is sampled by an analog-to-digital converter (A/D), encoded, modulated with multilevel FM, and then transmitted using frequency hopping techniques. The process is reversed at the receiver.

The noise-free FM signal with a slow FH scheme at the radio frequency (RF) is expressed as

$$x(t) = \sqrt{2S}e^{j[2\pi \int_{-\infty}^{t}(f_l+\beta s(t))\,dt]}, \tag{1}$$

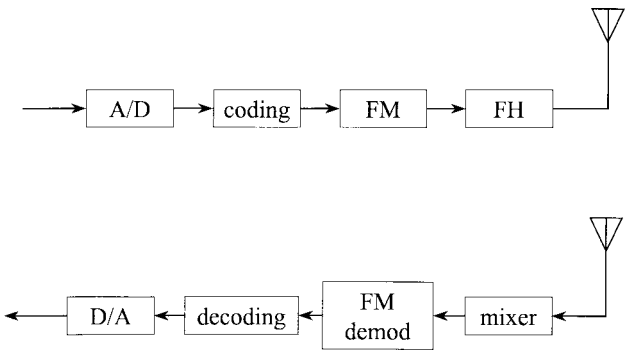

FIG. 1. Block diagram of an FH/FM system.

where S is the transmit power, f_l is the hopping frequency, $s(t)$ is the signal input, and β is the modulation factor. If $s(t)$ is a digital signal and its lth data symbol is described as $b_l \in \{0, 1, \ldots, M\}$, then we can rewrite Eq. (1) as

$$x(t) = \sqrt{2S} \sum_{l=0}^{\infty} e^{j[2\pi(f_l + b_l f_d)t + \phi_l]} p_T(t - lT), \tag{2}$$

where T is the symbol duration, ϕ_l is the random phase for the lth data symbol, f_d is the frequency deviation, which denotes the frequency separation between two adjacent signal levels, and $p_T(t) = 1$ for $t \in (0, T)$ and zero, otherwise.

2.2. FM Threshold Effect

The SNR of an FM receiver is proportional to the carrier-to-noise (CNR) at high CNR. However, when the CNR becomes low, the SNR decreases sharply and the FM receiver breaks. This phenomenon is known as the FM threshold effect [1]. It is reported that the threshold effect in FM receivers may be avoided in most practical cases of interest if the CNR is equal to or greater than 20 (i.e., 13 dB) [1]. Therefore, the threshold value becomes a simple and yet a practically important parameter in FM receiver design. In this paper, we hence consider the probability that the CNR is equal to or greater than a certain threshold level. For the underlying problem, the threshold level corresponds to the signal power at the receiver of -115 dB m (i.e., 3.162×10^{-15} W) [2].

3. CHANNEL MODEL

3.1. Channel Model

In this section, we consider the channel model which involves a transmit antenna near the rotating blades. Figure 2 illustrates the communication environment.

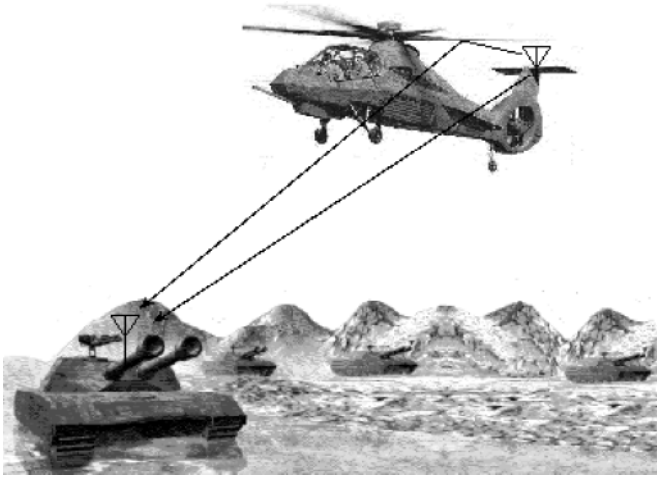

FIG. 2. Illustration of the environment.

To simplify the analysis, we make the following assumptions.

(A1) The transmitter and the receiver antennas are both modeled as electrically short dipoles whose length is much smaller than the wavelength.

(A2) The blades are considered as perfect conductors.

(A3) The width of a blade w is considered less than one quarter of a wavelength and much smaller than the length of the blade. In this case, each blade can be equivalently modeled as a wire with radius $a = w/4$. The mutual coupling effects among the blades are neglected.

(A4) Each blade is always visible to both the source and the airborne antenna; i.e., there is no shielding of the blades.

(A5) The time delay of the scattering paths compared with the direct path is much less than the symbol duration (or the reciprocal of the signal bandwidth).

By assuming a triangle current distribution on the transmitter antenna, the electrical near field transmitted from the transmitter antenna at (x_t, y_t, z_t) and received at a blade point $(x'(t), y'(t), z'(t))$ is expressed as [3]

$$\mathbf{E}_{inc}(x', y', z', t) = \mathbf{r}_t \eta \frac{I_t l_t}{4\pi r_t^2} \cos\theta \left[1 + \frac{1}{jkr_t}\right] e^{-jkr_t} + \boldsymbol{\theta}_t jk\eta \frac{I_t l_t}{8\pi r_t} \sin\theta \left[1 + \frac{1}{jkr_t} - \frac{1}{(kr_t)^2}\right] e^{-jkr_t}, \tag{3}$$

where $\mathbf{r}_t$ and $\boldsymbol{\theta}_t$ are the unit vectors along the propagation and elevation directions (with the origin of the axis coordinate at the center of the transmitter antenna), $\eta = 120\pi$ is the intrinsic impedance of free space, I_t and l_t are respectively the peak current magnitude and the length of the transmit antenna, $r_t = ((x' - x_t)^2 + (y' - y_t)^2 + (z' - z_t)^2)^{1/2}$ is the distance between the incident point at the blades to the transmitter antenna, $k(t) = 2\pi/\lambda(t)$ is the wave number, and $\lambda(t)$ is the wavelength at the carrier frequency, which changes at the hopping rate.

The electric voltage induced at an infinitesimal du of a blade can be expressed as

$$dv(x', y', z', t) = \mathbf{E}_{inc}(x', y', z', t) \cdot \mathbf{a}_m(t)\, du, \tag{4}$$

where $\mathbf{a}_m(t)$ is the unit vector along the mth blade and "$\cdot$" denotes the inner product between two vectors.

It is noted that some parameters, such as r, r_t, $\mathbf{r}_t$, θ, and $\boldsymbol{\theta}_t$, are the function of position of the incident point (x', y', z') and time t, although (x', y', z', t) is omitted for notation simplicity.

The current distribution on the blades can in principal be evaluated using the method of moments [4] based on (4). For computational efficiency, however, we have adopted an accurate closed-form expression given in [5, 6] for the current induced on a thin-wire antenna at an incident point (x, y, z) due to a delta-function voltage source at point (x', y', z'). Weighting that current by the incremental voltage du in (4) and integrating over the length of the blade thus results in the induced current distribution on the blade due to the incident field

in (3). Denote by I_m the current distribution over the mth blade; in the far-field receiver, the scattered field from the blade can be expressed as

$$\mathbf{E}_{sc}(t) \approx -j\omega\mu\mathbf{A} = -j\omega\mu \sum_{m=1}^{M} A_m \mathbf{a}_m$$

$$= -j\omega\mu \frac{e^{-jk(t)r_0}}{4\pi r_0} \sum_{m=1}^{M} \int_0^L I_m e^{jk(t)l\mathbf{a}_m \cdot \mathbf{r}_r} \mathbf{a}_m \, dl, \tag{5}$$

where μ is the magnetic permeability, $\mathbf{A}$ is the magnetic vector potential, $r_0 = (x_r^2 + y_r^2 + z_r^2)^{1/2}$ is the distance between the center of blades (coordinate origin) and the receiver located at (x_r, y_r, z_r), $r_r = ((x - x_r)^2 + (y - y_r)^2 + (z - z_r)^2)^{1/2}$ is the distance between the scattering point $(x(t), y(t), z(t))$ and the receiver located at (x_r, y_r, z_r), $\mathbf{r}_r$ is the unit vector at this direction, M is the number of blades, and L is the length of each blade.

On the other hand, the direct path from the transmitter antenna is expressed as

$$\mathbf{E}_{di}(t) = \boldsymbol{\theta}\, jk(t)\eta \frac{I_t l_t}{8\pi r_0} \sin\theta e^{-jk(t)r_0}, \tag{6}$$

where $\boldsymbol{\theta}$ is the unit norm vector along the θ direction. From (5) and (6), the received signal can be calculated by using the following equivalent aperture of a small dipole

$$S_{eq} = 3\lambda^2(t)/\eta. \tag{7}$$

Under assumption A5, the fading caused by the scattering and the Doppler effect can be considered as flat fading, and the received signal at the receiver becomes the summation of the contributions of the direct path and that of the scattering components from the blades.

3.2. Numerical Results

Channel impairments due to scatterings from rotating blades highly depend on the values assumed by the various parameters defining the channel model. In this section, we use the set of values listed in Table 1. It is important to note that the results and arguments presented below are based on these specific

TABLE 1

Major Parameters

Parameter	Notation	Used value
Transmit power	P_t	10 W
Radio frequency	$\omega_c/2\pi$	30–88 MHz
Symbol rate	$1/T$	16 kbauds
Hopping rate	f_h	110 hops/s
Frequency separation	Δf	25 kHz
Length of blades	L	7.5 m
Number of blades	M	4
Rotation speed	$\omega_r/2\pi$	4 r/s
Flight speed	v	200 mph

values and may change with the carrier frequency, the signal coding/modulation, and the rotorcraft structure and dimension.

Based on the values given in Table 1, $\omega_r T = 2\pi \times 4/(16 \times 10^3) = 1.57 \times 10^{-3}$ (rad) $= 0.09°$. Therefore, over one symbol period, the instantaneous Doppler frequency shift corresponding to a signal point on the blade remains approximately unchanged, since $\omega_r T$ is very small.

At the blade tips, the distance traveled over this period is $\omega_r T L = 1.57 \times 10^{-3} \times 7.5 \approx 1.18 \times 10^{-2}$ (m), which is much smaller than the wavelength (10–3.4 m at 30–88 MHz RF). Accordingly, the blades can be considered of fixed positions over a symbol period.

The maximum possible Doppler frequency is determined by the velocity of blade tips, $v_{\text{tip}} = \omega L$, and is given by

$$f_{D\max} = 2v_{\text{tip}}/\lambda = 2\omega L/\lambda \tag{8}$$

which is about 111 Hz at 88 MHz. The Doppler effect is not significant as $F_{D\max} T \approx 0.006$ is small [12].

3.2.1. Effects of elevation angle of the receiver antenna. From the signal model, the direct path from the transmitter antenna is dominated by vertical polarization, whereas the scattering component is dominated by horizontal polarization. Therefore, the signal at the receiver antenna will generally include both direct and scattering components. However, when the horizontal distance between the transmitter and the receiver is much larger than their height difference and the rotorcraft maintains a horizontal flight, increasing the elevation angle of the receiver antenna, θ_r, will reduce the direct path and enhance the scattering component.

We show in Figs. 3–6 the magnitudes of the direct and scattering components and their cumulative probabilities, for both angles $\theta_r = 45°$ and $85°$. Changes in the elevation angles are expected, as the receiver antenna is typically hand- or back-held by soldiers on the ground. Also, a rotorcraft may change its elevation angle, which results in a similar effect in the sense that the

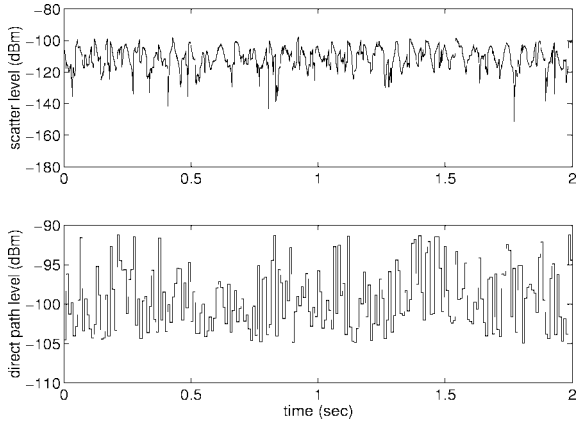

FIG. 3. Scatterings and direct path: $\theta_r = 45°$ at $(x_t, y_t, z_t) = (-9, 0, -3)$ m.

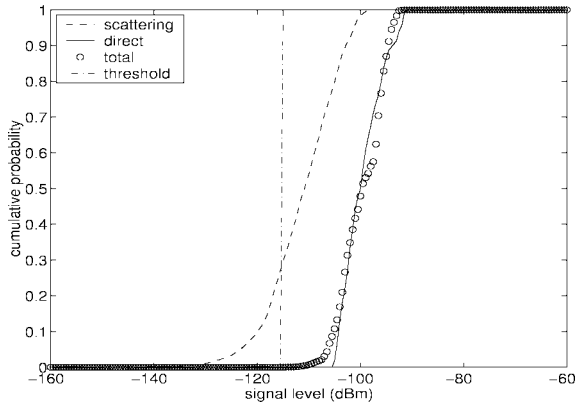

FIG. 4. Cumulative probability: $\theta_r = 45^\circ$ at $(x_t, y_t, z_t) = (-9, 0, -3)$ m.

polarization relationship between the transmitter and the receiver would vary. The transmitter antenna is located at the tail of the rotorcraft and positions at $(x_t, y_t, z_t) = (-9, 0, -3)$ m relative to the center of blades. The horizontal distance between the rotorcraft and the receiver is set equal to 50 km. In addition to the path loss, the results in Figs. 3–6 are adjusted by a power loss margin of 40–45 dB, depending on the employed frequencies. This figure is typical for normally encountered terrain shadowing and ground effects.

In Figs. 3 and 5, the magnitude variations of the direct path are due to the changes in the equivalent aperture at different hopping frequencies. The magnitude variations of the scattering component are further influenced by changes in signal polarizations and strengths due to the relative position between the transmitter antenna and the rotating blades.

For the $\theta_r = 45^\circ$ case, the direct path has a stronger level than the required threshold, and the scattering component is much weaker. Therefore, the combined received signal is dominated by the direct path, and the fading

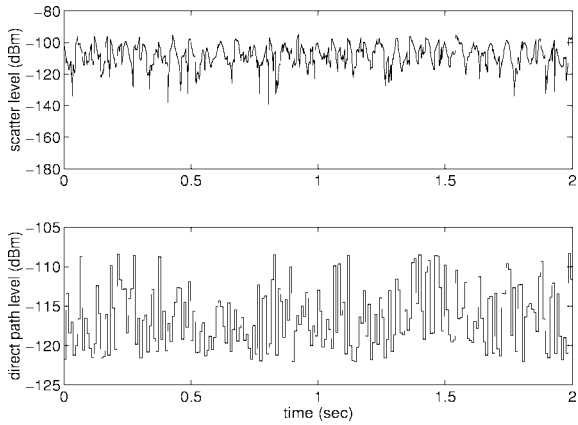

FIG. 5. Scatterings and direct path: $\theta_r = 85^\circ$ at $(x_t, y_t, z_t) = (-9, 0, -3)$ m.

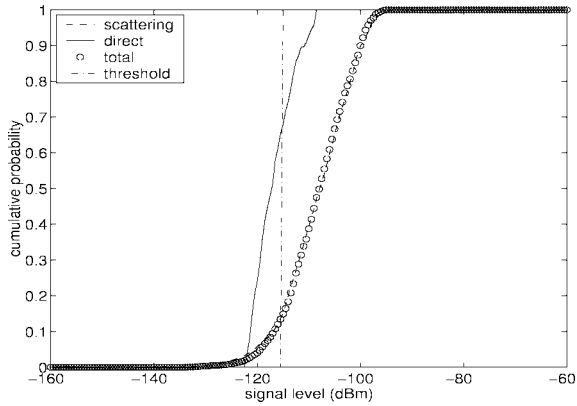

FIG. 6. Cumulative probability: $\theta_r = 85^\circ$ at $(x_t, y_t, z_t) = (-9, 0, -3)$ m.

effect of the scattering component is negligible. On the other hand, for the $\theta_r = 85^\circ$ case, the level of the direct path is relatively low and it cannot alone provide the desired communication quality. In this case, the average level of the scattering component is comparable to or even stronger than the direct path. The probability that the signal level is smaller than the threshold is almost 14%, which fails to deliver high quality signal communications.

3.2.2. Effects of the position of transmitter antenna. In this section, we examine how the position of the transmitter antenna changes the channel characteristics. Figures 7 and 8 depict the results for a different position of the transmitter antenna: $(x_t, y_t, z_t) = (-1, 0, -1)$ m relative to the center of blades, with $\theta_r = 85^\circ$. Although the change in antenna position virtually does not bring about any difference for the direct path, the scattering component level becomes much stronger as the transmitter antenna moves closer to the blades. As a result, the probability that the signal level is weaker than the threshold drops to 2.6%. However, this outage probability is still considered

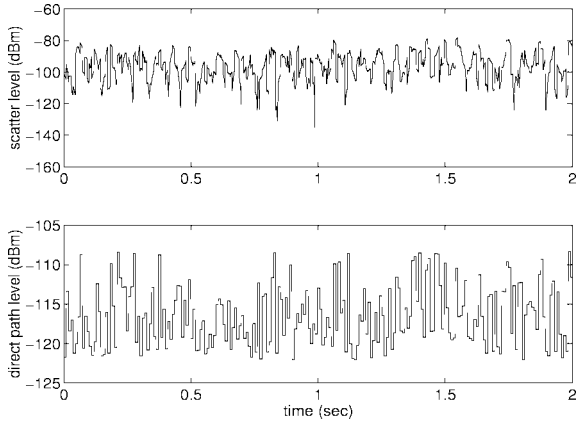

FIG. 7. Scatterings and direct path: $\theta_r = 85^\circ$ at $(x_t, y_t, z_t) = (-1, 0, -1)$ m.

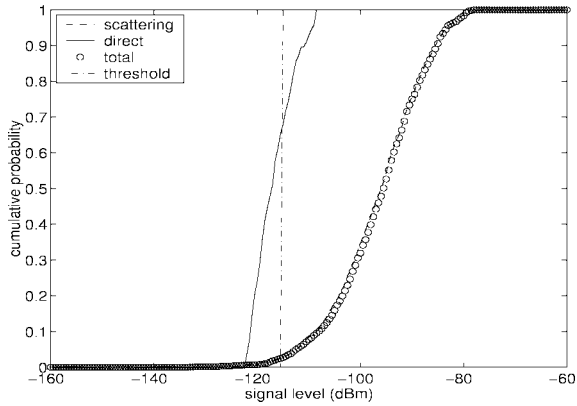

FIG. 8. Cumulative probability: $\theta_r = 85^\circ$ at $(x_t, y_t, z_t) = (-1, 0, -1)$ m.

unacceptable. Diversity techniques are applied in the next section to further reduce this probability.

As can be seen from the cumulative probability in Figs. 4, 6, and 8, the scattering component is in general not Rayleigh. Also, it is worth mentioning that reflection and diffraction by the rotorcraft body or terrain may further alter the signal polarization and subsequently the power ratio between the direct path and the scattering component. The power ratio can also be changed when the line-of-sight between the transmitter and the receiver antennas is shadowed.

4. DIVERSITY TECHNIQUES

Diversity techniques are effective means to reduce the effect of flat fading. In this section, we examine the applicability and compare the performance of different diversity techniques, namely, the transmitter diversity which uses multiple transmitter antennas, and the two cases of MCFH and FFH, which both utilize the weakly correlated channel characteristics of different hopping frequencies.

Herein, we consider $\theta_r = 85^\circ$, which presents significant signal fading in which scatterings are stronger than the direct path. The transmitter antennas are located close to the center of blades to ensure the communication quality.

4.1. Transmitter Diversity with Differential Space–Time Codes

Transmitter diversity techniques fully exploit the spatial diversity offered by multiple transmitter antennas, leading to improved overall performance of wireless communication systems [8, 9]. However, these methods are based on the assumption that the perfect channel state information is available at the receiver, or at least can be accurately estimated by, for example, transmitting training sequences. The fast time-varying channel and the periodic change of the hopping frequency make channel knowledge or estimation infeasible.

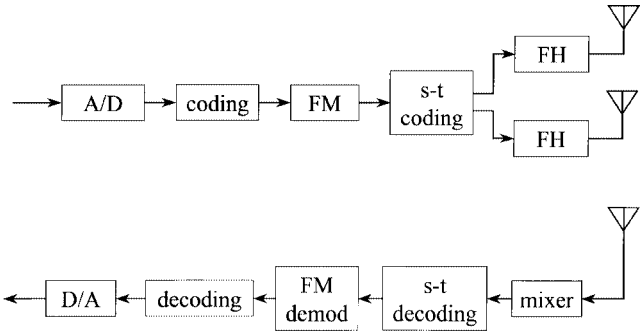

FIG. 9. Block diagram of the FH/FM system with transmitter diversity.

To overcome the channel knowledge constraint, differential space–time coding (DSTC) techniques can be used [10, 11]. Although the performance of differential space-time coding techniques is inferior to that of the conventional space–time coding techniques when the channel characteristics are available, it is nevertheless effective in the underlying problem. Figure 9 shows the block diagram of the FH/FM communication system with the use of transmitter diversity techniques. It is noted that, to avoid the nonlinearity of FM which causes difficulty in applying transmitter diversity to the underlying problem, we perform space–time coding after the FM modulation and decode the signal before the FM demodulation.

If we ignore the block-by-block changes of the channel coefficient vector $\mathbf{h} = [h_1, \ldots, h_Q]^{\mathrm{T}}$ (this assumption is reasonable when the block size Q is much smaller than the coherence time of the channels which is approximately one hopping period), then the combined channel coefficient becomes

$$C_t = \|\mathbf{h}\|^2/Q = \sum_{q=1}^{Q} |h_q|^2/Q. \tag{9}$$

The factor $1/Q$ is used to normalize the transmitter power at each antenna so that the total transmitter power remains equal to the single antenna case. However, the threshold in the transmitter diversity case should rise to -112 dB m, due to the 3-dB noise enhancement in performing differential decoding [11].

The two antennas ($Q = 2$) are located at $(x_t, y_t, z_t) = (-1, 0, -1), (0, -1, -1)$ m. The respective channels are shown in Figs. 7–8 and 10–11. It is noted that different positions of a transmitter antenna may demonstrate different statistical characteristics. Therefore, to achieve good diversity gain, it is important to choose antenna positions so that the channel envelopes of different transmitter antennas have similar statistical characteristics and small correlation.

The cumulative probability of the output power after diversity combining is illustrated in Fig. 12. In this figure, "threshold 1" (-115 dB m) refers to the threshold value corresponding to the single antenna curve, whereas "threshold 2" (-112 dB m) corresponds to the combined signal curve. The probability that the combined signal level is weaker than threshold 2 is 0.7%.

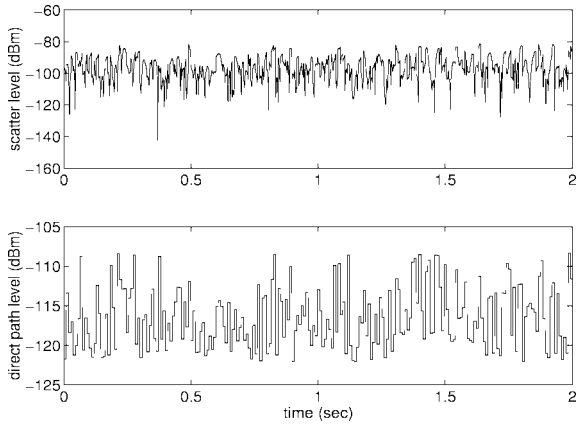

FIG. 10. Scatterings and direct path: $\theta_r = 85^\circ$ at $(x_t, y_t, z_t) = (0, -1, -1)$ m.

4.2. MCFH and FFH Diversities

MCFH is a direct application of conventional frequency diversity in FH that transmits the same signal at multiple frequencies. At the receiver, the signals transmitted at different frequencies are received and combined. In this case, diversity gain can be achieved without the need for multiple antennas at either the transmitter or the receiver. Signals at different frequencies can, therefore, be received without interference. Figure 13 shows the block diagram of the MCFH diversity system.

In FH systems, the frequency diversity gain can also be realized by using FFH, which has the same structure as that of slow FH, shown in Fig. 1. The only key difference between slow and fast FH schemes is that, in FFH, the hopping rate is higher than the symbol rate. As a result, the signal power of one symbol spreads over different hopping frequencies.

The FFH, compared to the MCFH, has a narrower chip period. Subsequently, FFH is more sensitive to the channel delay spread, but is more immune to

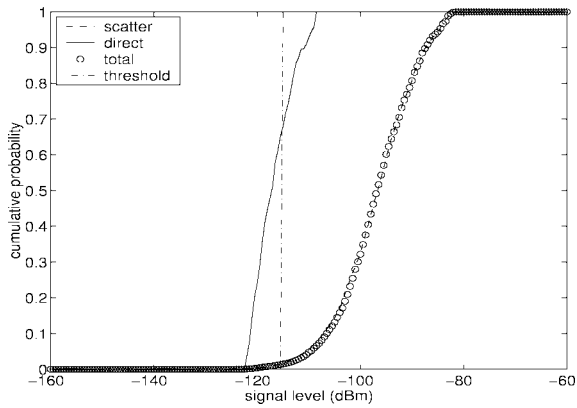

FIG. 11. Cumulative probability: $\theta_r = 85^\circ$ at $(x_t, y_t, z_t) = (0, -1, -1)$ m.

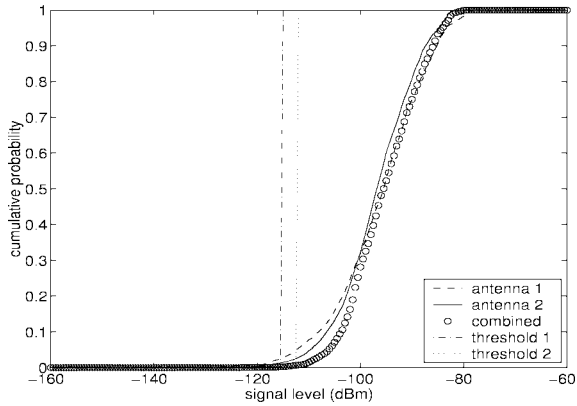

FIG. 12. Cumulative probability of the transmitter diversity system.

the Doppler effect [12]. However, in the underlying problem, the delay spread (the maximum time delay between the direct path and the delayed path is 57 ns ≈ 0.0009 T) and the Doppler spread (when $F_d = 100$ Hz, $F_d T \approx 0.006$) are both negligible.

For MCFH, denote h_q $(q = 1, \ldots, Q)$ as the channel coefficient of the qth frequency. Then, the received signal at the qth hopping frequency is given by

$$r_q(t) = \sqrt{2S/Q} h_q \sum_{l=0}^{\infty} e^{j[2\pi(f_{l,q}+b_l f_d)t+\phi_{l,q}]} p_T(t - lT). \tag{10}$$

On the other hand, for FFH, h_q $(q = 1, \ldots, Q)$ represents the channel coefficient of the qth hop $(QT_h = T)$. The received signal at the qth hopping frequency is, therefore,

$$r_q(t) = \sqrt{2S} h_q \sum_{l=0}^{\infty} e^{j[2\pi(f_{l,q}+b_l f_d)t+\phi_{l,q}]} p_{T_h}(t - lT - qT_h). \tag{11}$$

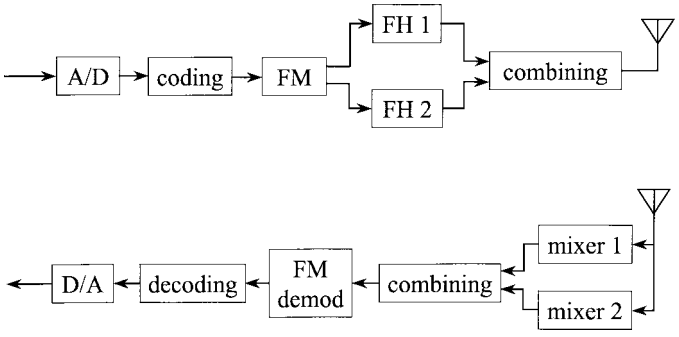

FIG. 13. Block diagram of the FH/FM system with frequency diversity.

When the optimum combining rule is applied, the output signals are, respectively,

$$r(t) = \sqrt{2S/Q} \sum_{q=1}^{Q} |h_q|^2 \sum_{l=0}^{\infty} e^{j[2\pi(f_{l,q}+b_l f_d)t+\phi_{l,q}]} p_T(t - lT) \qquad \text{(MCFH)} \qquad (12)$$

and

$$r(t) = \sqrt{2S} \sum_{q=1}^{Q} |h_q|^2 \sum_{l=0}^{\infty} e^{j[2\pi(f_{l,q}+b_l f_d)t+\phi_{l,q}]} p_{T_h}(t - lT - qT_h) \qquad \text{(FFH)} \qquad (13)$$

In both cases, the combined channel coefficient becomes

$$C_{mc} = C_f = \|\mathbf{h}\|^2 = \sum_{q=1}^{Q} |h_q|^2. \qquad (14)$$

In the simulations, we use two different frequencies ($Q = 2$) for both MCFH and FFH. The transmitter antenna is positioned at $(x_t, y_t, z_t) = (-1, 0, -1)$ m and $\theta_r = 85°$. The frequency difference between the two frequency carrier is chosen to be 29 MHz. Figures 14 and 15 show the channel characteristics for one FFH realization, where $T_h = T/2$. The cumulative probability of the output power for both MCFH and FFH is illustrated in Figs. 16 and 17, respectively. The difference between the two figures is due to the fact that the FFH undergoes more frequency hops than the MCFH does during the same period. For both MCFH and FFH, there is no observation that the combined signal level is weaker than the required threshold.

It is noted that MCFH can be used in the transmitter diversity with DSTC, whereas for the FFH it would be difficult to do so because the channel changes rapidly with the fast hopping.

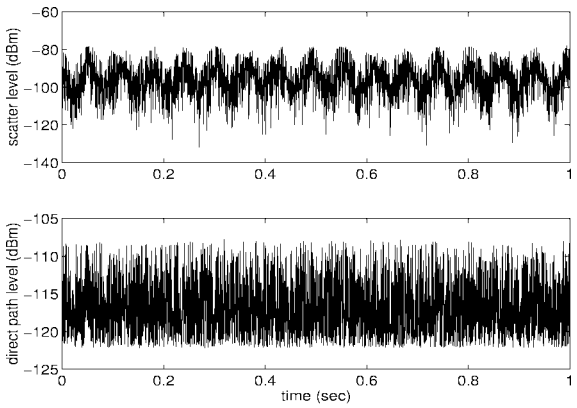

FIG. 14. Scatterings and direct path for FFH: $\theta_r = 85°$ at $(x_t, y_t, z_t) = (-1, 0, -1)$ m.

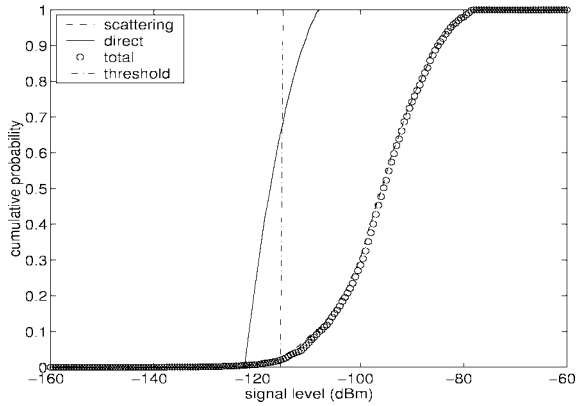

FIG. 15. Cumulative probability for FFH: $\theta_r = 85^\circ$ at $(x_t, y_t, z_t) = (-1, 0, -1)$ m.

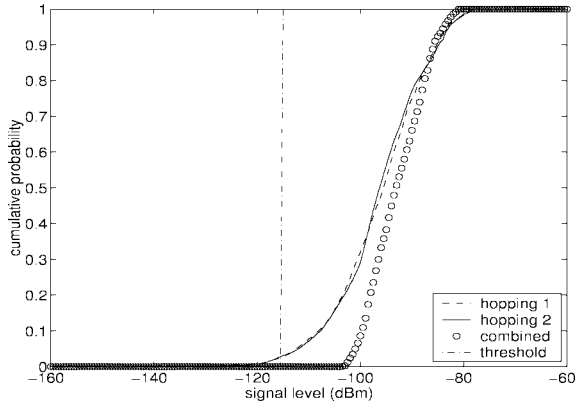

FIG. 16. Cumulative probability of the MCFH system.

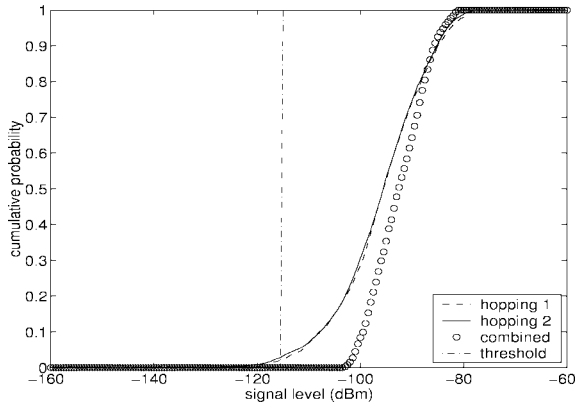

FIG. 17. Cumulative probability of the FFH system.

5. CONCLUSION

In this paper, diversity techniques are applied to combat fading caused by the rotating blades on a rotorcraft. The wireless communication channel models for rotorcrafts are developed, including the near-field effects. It is shown that the scattering component is not Rayleigh distributed, and the power ratio of the direct path and the scattering component is sensitive to elevation angle of the receiver antenna, the distance between the transmitter antenna and the blades, and the elevation angle between them. When the scattering component has comparable or higher power than the direct path, significant fading occurs.

Based on the devised channel models, the applicability of transmitter and frequency diversity techniques, namely, transmitter diversity, MCFH, and FFH, have been examined and shown to mitigate fading due to the rotating blades. Although all diversity techniques reduce fading, the offerings of transmitter diversity are more sensitive to antenna locations to the extent that it becomes less attractive than MCFH and FFH techniques. The latter are shown to provide higher diversity gain for the antenna locations used.

REFERENCES

1. Haykin, S., *Communication Systems.* Wiley, New York, 1978.
2. Nachamkin, J., the Boeing Company, personal communications.
3. Balanis, C., *Antenna Theory—Analysis and Design,* 3rd ed. Wiley, New York, 1997.
4. Harrington, R. F., *Field Computation by Moment Methods.* Macmillan, New York, 1968.
5. Hoorfar, A. and Chang, D. C., Analytic determination of the transient response of a thin-wire antenna based upon an SEM representation. *IEEE Trans. Antennas Propagat.* **30** (1982), 1145–1152.
6. Rispin, L. W. and Chang, D. C., Wire and loop antennas. In *Antenna Handbook: Theory, Application and Design* (Lo, Y. T. and Lee, S. W., Eds.). Van Nostrand Reinhold, New York, 1988.
7. Zhang, Y., Amin, M. G., and Mancuso, V., On the effects of rotating blades on DS/SS communication systems. In *Proc. IEEE Workshop on Statistical Signal and Array Processing*. pp. 682–686, Pocono Manor, PA, Aug. 2000.
8. Alamouti, S. M., A simple transmit diversity technique for wireless communications. *IEEE J. Selected Areas Commun.* **16** (1998), 1451–1459.
9. Tarokh, V., Seshadri, N., and Calderbank, A. R., Space–time codes for high data rate wireless communications: performance criteria an code construction. *IEEE Trans. Info. Theory* **44** (1998), 744–765.
10. Hughes, B. L., Differential space–time modulation. *IEEE Trans. Inform. Theory* **46** (2000), 2567–2578.
11. Hochwald, B. M. and Sweldens, W., Differential unitary space–time modulation. *IEEE Trans. Commun.* **48** (2000), 2041–2052.
12. Shin, O.-S. and Lee, K. B., Performance comparison of FFH and MCFH spread-spectrum systems with optimum diversity combining in frequency-selective Rayleigh fading channels. *IEEE Trans. Commun.* **49** (2001), 409–416.

MOENESS AMIN received his B.Sc. from Cairo University in 1976, M.Sc. from University of Petroleum and Minerals in 1980, and Ph.D. in electrical engineering in 1984 from University of

Colorado, Boulder. He has been on the faculty of the Department of Electrical and Computer Engineering at Villanova University since 1985, where he is now a professor. From 1995 to 1997, he was an associate editor of the *IEEE Transactions on Signal Processing* and a member of the Technical Committee of the IEEE Signal Processing Society on Statistical Signal and Array Processing. He is currently a member of the IEEE Signal Processing Society Technical Committee on Signal Processing for Communications. He was the General Chair of the 1994 IEEE International Symposium on Time-Frequency and Time-Sale Analysis and the General Chair of the 2000 IEEE Workshop on Statistical Signal and Array Processing. Dr. Amin is the recipient of the 1997 IEEE Philadelphia Section Service Award and the IEEE Third Millennium Medal. He is also the recipient of the 1997 Villanova University Outstanding Faculty Research Award. He serves on the Committee of Science and Arts of the Franklin Institute. His current research interests are in the areas of time-frequency analysis, spread spectrum communications, smart antennas, and blind signal processing. Dr. Amin is a fellow of IEEE.

YIMIN ZHANG received his M.S. and Ph.D. from the University of Tsukuba, Japan, in 1985 and 1988, respectively. He joined the faculty of the Department of Radio Engineering, Southeast University, Nanjing, China, in 1988. He served as a technical manager at Communication Laboratory Japan, Kawasaki, Japan, from 1995 to 1997, and a visiting researcher at ATR Adaptive Communications Research Laboratories, Kyoto, Japan, from 1997 to 1998. Currently, he is a research fellow with the Department of Electrical and Computer Engineering, Villanova University, Villanova, PA. His current research interests are in the areas of array signal processing, space-time adaptive processing, multiuser detection, blind signal processing, digital mobile communications, and time-frequency analysis. Dr. Zhang is a senior member of IEEE.

VINCENT MANCUSO is a senior staff engineer at Boeing in Philadelphia, PA. He is primarily responsible for electromagnetic effects analysis and design. He received a B.S.E.E. from Pennsylvania State University in 1983 and a M.S.E.E. from Fairleigh Dickinson University in 1991. He has published articles on electromagnetic effects on communication and radar equipment. Previously he worked for ARINC, AEL, and General Electric.

AHMAD HOORFAR received his B.S.E.E. from the University of Tehran, Iran, in 1975, and an M.S. and a Ph.D. in electrical engineering from the University of Colorado at Boulder, in 1978 and 1984, respectively. From 1984 to 1986 he was a post-doctoral research associate in the Electromagnetics Laboratory at the University of Colorado. In 1986 he became a research faculty in the NSF center for Microwave/Millimeter-waves Computer-Aided Design (MIMICAD) in Boulder. Since 1988 he has been with Villanova.